

# Verifying the ACIS Contamination Model with 1E0102.2-7219

Joseph M. DePasquale<sup>a</sup>, Paul P. Plucinsky<sup>a</sup>, Alexey A. Vikhlinin<sup>a</sup>, Herman L. Marshall<sup>b</sup>,  
Norbert S. Schulz<sup>b</sup>, Richard J. Edgar<sup>a</sup>

<sup>a</sup>Harvard-Smithsonian Center for Astrophysics, 60 Garden St, Cambridge, MA, USA;

<sup>b</sup>MIT Center for Space Research, 77 Massachusetts Avenue, Cambridge, MA, USA

## ABSTRACT

The low-energy sensitivity of the Advanced CCD Imaging Spectrometer (ACIS) instrument on board the *Chandra* X-ray Observatory (CXO) has been continuously degrading since launch due to the accumulation of a layer of contamination on the ACIS optical blocking filter (OBF). This contamination layer, the result of out-gassing and off-gassing within the observatory, introduces a new, energy dependent absorption into the ACIS response. The thickness of this layer has been increasing with time and its spatial distribution across the OBF has been continually changing with time. We utilize multiple observations of the SMC Supernova Remnant 1E0102.2-7219 to verify the models for the spectral, temporal, and spatial dependence of the contamination layer. We also use this source to investigate cross-calibration between the front illuminated (FI) and back illuminated (BI) CCDs. 1E0102.2-7219 has a soft, line-dominated spectrum which is very sensitive to the additional absorption of the contamination layer. The extensive calibration observations of 1E0102.2-7219 over the course of the mission at several different locations on the ACIS Imaging (I) and Spectroscopy (S) arrays allows for a verification of the temporal and spatial dependence of the contamination model.

**Keywords:** Chandra, space missions, contamination, CCD calibration, low energy sensitivity

## 1. INTRODUCTION

As of 23 July 2004, the *Chandra* X-ray Observatory (CXO) has been in Earth orbit for 5 years, and has observed over 4300 astrophysical sources. As one of NASA's *Great Observatories*, *Chandra* continues to provide some of the most exquisitely sensitive X-ray observations to the astronomical community. Maintaining accurate calibration of *Chandra's* instruments is of paramount importance to the observatory's mission.

The contamination of the ACIS OBF, first noticed in late 1999,<sup>1</sup> has been the main focus of recent calibration efforts. Marshall *et al.* have shown that, using high resolution spectroscopy of bright sources taken with the Chandra Low Energy Transmission Grating Spectrometer (LETGS), an accurate determination of the composition of the contaminant can be made by analyzing absorption edges.<sup>2</sup> Gratings data have shown that the contaminant is largely comprised of carbon, with smaller amounts of O and F. Figure 1 shows the obvious effects that this contamination layer has had on the measured count rate of E0102 on the I3 and S3 chips. The decline in count rate over time in both plots is indicative of a continually growing contamination layer, while the consistent node-to-node variations seen in the I3 figure clearly illustrate the spatial dependence of the contamination.

Utilizing the gratings data and External Calibration Source (ECS) data, Vikhlinin has developed a model of the contaminant, incorporating temporal, energy and spatial dependencies. The ECS data, being taken at more

---

Further author information: (Send correspondence to J.M.D.)

J.M.D.: E-mail: jdepasquale@cfa.harvard.edu

Copyright 2004 Society of Photo-Optical Instrumentation Engineers.

This paper was published in *High Energy Detectors in Astronomy*, Andrew D. Holland, Editor, Proceedings of SPIE Vol. 5501, p. 328, and is made available as an electronic reprint with permission of SPIE. One print or electronic copy may be made for personal use only. Systematic or multiple reproduction, distribution to multiple locations via electronic or other means, duplication of any material in this paper for a fee or for commercial purposes, or modification of the content of the paper are prohibited.

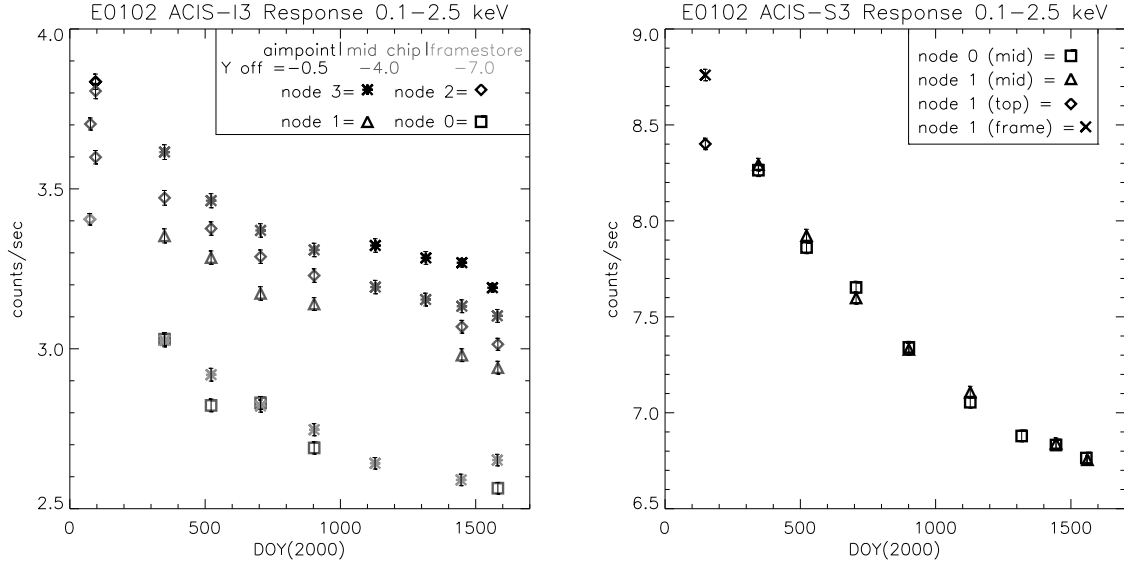


**Figure 1.** The left panel shows the E0102 count rate (0.1 - 2.5 keV) at each observation on I3; the same plot is shown on the right panel for S3 E0102 observations.

regular intervals, and at more locations than gratings data, are a natural source for examining the spatial and time dependence of the contamination layer. As detailed in Vikhlinin’s internal CXC memo,<sup>3</sup> the ratio of the ECS spectral line fluxes of Mn+Fe L and Mn-K $\alpha$  should be time independent, as they are derived from the same source. The count rate at the L-lines (around 0.67 keV) is severely affected by contamination, while the Mn-K line (around 5.898 keV) is not. Measurements of the change of the L/K ratio provide insight into the optical depth of the contaminant at low energies in time and position.

In this paper, we investigate the fidelity of the current Chandra contamination model by examining both its time and spatial dependencies through analysis of ACIS-I and ACIS-S observations of E0102.2-7219. In Section 2, we detail the steps involved in spectral processing and extraction. A description of the spectral model used in this analysis is presented in section 2.2, along with a brief description of the contamination model. Our analysis methods and results are presented in section 3.1, along with a brief discussion of the FI vs. BI agreement. Finally, in section 4 we summarize our findings and look to the future of calibration of the ACIS contamination layer.

## 2. DATA PREPARATION

### 2.1. Spectral Processing & Extraction

Table 1 summarizes the dates and locations of the 62 observations of E0102 on I3 and S3 that we have used. Though the same analysis tools are utilized, ACIS-I and ACIS-S data require slightly different processing routines due to the fact that the CTI correction algorithm can only be applied to the ACIS-I data. We begin processing ACIS-I data by running the CXC CTI correction via the *CIAO* tool, *acis\_process\_events*, on the level 1 events file. This same tool is applied to ACIS-S data without CTI correction. For both ACIS-I and S data, we filter the events file on good *ASCA* grades, good time interval (gti) and chip number to create the level 2 events file. Vikhlinin’s *apply\_gain* is then applied to the level 2 events file to adjust the time dependence of the gain. Another *CIAO* tool, *acispec*, is used to extract the spectrum in PI channels with the source and background regions defined in the visualization tool, *DS9*. Once spectral extraction is complete, Vikhlinin’s analysis tools, *calcrmf2* and *calcarf*, are run to compute a new weighted rmf and an arf file that incorporates the spatial and

time dependent contamination model. Work is currently underway to include these two analysis tools as standard processing tools in an upcoming *CIAO* release. The default, weighted *rmf* and *arf* created during extraction are used to compare the test results to the default results. It should also be mentioned that in the course of this analysis, the time-dependent contamination correction has been incorporated into the *Chandra CALDB* version 2.26 release; the spatially-dependent correction is still under development.

**Table 1. E0102 I3 & S3 Observations**

I3				S3			
Obsid	Date (DOY)	Y offset	Z offset	Obsid	Date (DOY)	Y offset	Z offset
0440	2000-04-04	-0.5	2.5	0141	2000-05-28	-1.0	2.0
0439	2000-04-04	-2.25	2.5	1702	2000-05-28	-1.0	-2.0
0136	2000-03-16	-4.0	2.5				
0140	2000-04-04	-5.5	2.5				
0420	2000-03-14	-7.0	2.5				
1313	2000-12-15	-7.0	0.5	1308	2000-12-10	1.0	0.0
1314	2000-12-15	-4.0	0.5	1311	2000-12-10	-1.0	0.0
1315	2000-12-15	-4.0	2.5				
1316	2000-12-15	-4.0	4.5				
1317	2000-12-15	-4.0	6.5				
1533	2001-06-05	-7.0	0.5	1530	2001-06-06	1.0	0.0
1534	2001-06-05	-4.0	0.5	1531	2001-06-06	-1.0	0.0
1535	2001-06-05	-4.0	2.5				
1536	2001-06-05	-4.0	4.5				
1537	2001-06-05	-4.0	6.5				
2835	2001-12-05	-7.0	0.5	2843	2001-12-06	1.0	0.0
2836	2001-12-05	-4.0	0.5	2844	2001-12-06	-1.0	0.0
2837	2001-12-05	-4.0	2.5				
2838	2001-12-05	-4.0	4.5				
2839	2001-12-05	-4.0	6.5				
2857	2002-06-21	-7.0	0.5	2850	2002-06-19	1.0	0.0
2858	2002-06-21	-4.0	0.5	2851	2002-06-19	-1.0	0.0
2859	2002-06-21	-4.0	2.5				
2860	2002-06-21	-4.0	4.5				
2861	2002-06-21	-4.0	6.5				
3535	2003-02-01	-7.0	0.5	3519	2003-02-01	1.0	0.0
3536	2003-02-02	-4.0	0.5	3520	2003-02-01	-1.0	0.0
3537	2003-02-02	-0.5	0.5				
3526	2003-08-06	-7.0	0.5	3544	2003-08-10	1.0	0.0
3527	2003-08-07	-4.0	0.5	3545	2003-08-08	-1.0	0.0
3528	2003-08-09	-0.5	0.5				
5146	2003-12-16	-7.0	0.5	5123	2003-12-15	1.0	0.0
5147	2003-12-19	-4.0	0.5	5124	2003-12-15	-1.0	0.0
5148	2003-12-19	-0.5	0.5	5251	2003-12-24	-1.0	0.0
5149	2003-12-19	-4.0	2.5	5252	2003-12-24	1.0	0.0
5150	2003-12-19	-4.0	4.5				
5137	2004-04-28	-7.0	0.5	5130	2004-04-09	-1.0	0.0
5139	2004-04-10	-0.5	0.5	5131	2004-04-05	1.0	0.0
5138	2004-04-28	-4.0	0.5				
5140	2004-04-30	-4.0	2.5				
5141	2004-04-30	-4.0	4.5				
5142	2004-04-30	-4.0	6.5				

## 2.2. Spectral & Contamination Models

The spectral model used in this analysis is comprised of a two-component absorption (*phabs* for galactic and *vphabs* for the Small Magellanic Cloud (SMC)), a thermal Bremsstrahlung for the continuum and 24 Gaussians to characterize the line emission. Data from *HETG*<sup>4</sup> and *XMM RGS*<sup>5</sup> are used to identify the strongest lines in the spectrum; line wavelengths, descriptions, and peak emissivities are taken from Astrophysical Plasma Emission Database of Smith *et al.* (see “[hea-www.harvard.edu/APEC/](http://hea-www.harvard.edu/APEC/)”). In most cases of fitting the I3 data, the normalizations of all line energies are allowed to float freely during fitting in the *XSPEC* spectral analysis package, with the exception of the 5 observations near the aimpoint of I3 where the 665 eV OVII line normalization is constrained to be 10 % of the 654 eV OVIII Ly  $\alpha$  line normalization. This same constraint was placed on all fits to the S3 data. The near aimpoint observations on I3 and the S3 observations suffer from degraded spectral resolution due to CTI effects. This added constraint prevents the fit from placing too much flux in the 665 eV line, which artificially lowers the flux of the 654 eV line. Table 2 shows the included lines used in the model.

**Table 2. E0102 Spectral Model: Included Lines**

$\lambda$ (Å)	Energy (keV)	Line Description	T of Peak Emissivity (K)	Peak Emissivity photons $\text{cm}^3 \text{s}^{-1}$
22.100	0.561	O7 $1s^2(^1S_0) - 1s2s(^3S_1)$ [For]	$2.00 \times 10^6$	$2.31 \times 10^{-15}$
21.600	0.574	O7 $1s^2(^1S_0) - 1s2p(^1P_1)$ [Res]	$2.00 \times 10^6$	$3.52 \times 10^{-15}$
18.970	0.654	O8 $1s(^2S_{1/2}) - 2p(^2P_{n/2})$ [Ly $\alpha$ ]	$3.16 \times 10^6$	$3.54 \times 10^{-15}$
18.627	0.665	O7 $1s^2(^1S_0) - 1s3p(^1P_1)$	$2.00 \times 10^6$	$3.74 \times 10^{-16}$
17.770	0.698	O7 $1s^2(^1S_0) - 1s4p(^1P_1)$	$2.51 \times 10^6$	$9.82 \times 10^{-17}$
16.010	0.774	O8 $1s(^2S_{1/2}) - 3p(^2P_{n/2})$ [Ly $\beta$ ]	$3.16 \times 10^6$	$4.00 \times 10^{-16}$
15.180	0.817	O8 $1s(^2S_{1/2}) - 4p(^2P_{n/2})$ [Ly $\gamma$ ]	$3.16 \times 10^6$	$1.20 \times 10^{-16}$
14.821	0.837	O8 $1s(^2S_{1/2}) - 5p(^2P_{n/2})$ [Ly $\delta$ ]	$3.16 \times 10^6$	$5.24 \times 10^{-17}$
13.700	0.905	Ne9 $1s^2(^1S_0) - 1s2s(^3S_1)$ [For]	$3.98 \times 10^6$	$2.10 \times 10^{-16}$
13.447	0.923	Ne9 $1s^2(^1S_0) - 1s2p(^1P_1)$ [Res]	$3.98 \times 10^6$	$4.11 \times 10^{-16}$
12.135	1.022	Ne10 $1s(^2S_{1/2}) - 2p(^2P_{n/2})$ [Ly $\alpha$ ]	$5.01 \times 10^6$	$3.36 \times 10^{-16}$
11.560	1.073	Ne9 $1s^2(^1S_0) - 1s3p(^1P_1)$	$3.98 \times 10^6$	$4.79 \times 10^{-17}$
11.000	1.127	Ne9 $1s^2(^1S_0) - 1s4p(^1P_1)$	$3.98 \times 10^6$	$1.25 \times 10^{-17}$
10.765	1.150	Ne9 $1s^2(^1S_0) - 1s5p(^1P_1)$	$3.98 \times 10^6$	$5.05 \times 10^{-18}$
10.239	1.212	Ne10 $1s(^2S_{1/2}) - 3p(^2P_{n/2})$ [Ly $\beta$ ]	$6.31 \times 10^6$	$4.27 \times 10^{-17}$
9.709	1.277	Ne10 $1s(^2S_{1/2}) - 4p(^2P_{n/2})$ [Ly $\gamma$ ]	$6.31 \times 10^6$	$1.33 \times 10^{-17}$
9.314	1.331	Mg11 $1s^2(^1S_0) - 1s2s(^3S_1)$ [For]	$6.31 \times 10^6$	$5.28 \times 10^{-17}$
9.169	1.352	Mg11 $1s^2(^1S_0) - 1s2p(^1P_1)$ [Res]	$6.31 \times 10^6$	$1.12 \times 10^{-16}$
8.422	1.473	Mg12 $1s^2(^1S_0) - 2p(^2P_{n/2})$ [Ly $\alpha$ ]	$7.94 \times 10^6$	$7.04 \times 10^{-17}$
7.850	1.579	Mg11 $1s^2(^1S_0) - 1s3p(^1P_1)$	$6.31 \times 10^6$	$1.31 \times 10^{-17}$
7.310	1.696	Mg11 $1s^2(^1S_0) - 1s5p(^1P_1)$	$6.31 \times 10^6$	$1.38 \times 10^{-18}$
6.740	1.840	Si13 $1s^2(^1S_0) - 1s2s(^3S_1)$ [For]	$1.00 \times 10^7$	$3.54 \times 10^{-17}$
6.183	2.006	Si14 $1s^2(^1S_0) - 2p(^2P_{n/2})$ [Ly $\alpha$ ]	$1.58 \times 10^7$	$4.95 \times 10^{-17}$
5.218	2.375	Si14 $1s^2(^1S_0) - 3p(^2P_{n/2})$ [Ly $\beta$ ]	$1.58 \times 10^7$	$6.80 \times 10^{-18}$

The contaminant is assumed to be comprised mainly of carbon, and is most likely a mixture of materials out-gassing and/or off-gassing from the spacecraft. The presence of F in the contaminant may suggest that radiation damaged, fluorocarbon-based compounds such as Braycote 601 and Krytox, both used in *Chandra* mechanisms, could contribute to the contamination.<sup>2</sup> The thickness of the contaminant is continually changing throughout the mission; calibration observations have shown the time dependence of the layer as well as the spatial non-uniformity. The spatial distribution of the contaminant matches the temperature profile predicted by thermal models of the ACIS filter.<sup>3</sup> The contamination layer is thicker along the outer edges of the OBFs, which are colder, and thinner in the middle of the OBFs, where the OBFs are warmer. It is assumed that the

contaminant is only collecting on the OBFs and not on the CCDs themselves as this would introduce a change in the CCD thermal properties such that an operating temperature of -120 C could not be maintained, which is not the case. The absorption imparted by the contaminant is most notable below 1 keV.

### 3. ANALYSIS & RESULTS

#### 3.1. Analysis Methods

Analysis of the processed data is grouped into two general categories, ACIS-I and ACIS-S data. The ACIS-I analysis consists of evaluating spectral fit results for both the default *CIAO* detector response files, and the contamination corrected response files. More specifically, we compare data with the time-dependent gain correction applied to data with the time-dependent gain correction and contamination correction, including spatial dependence. For ACIS-S data, we compare data processed with the default *CIAO* S3 QE curve and the time-dependent gain correction applied to data with the time-dependent gain correction and contamination correction including spatial dependence and a new prototype S3 QE curve currently in testing.

Each data set is loaded into *XSPEC* with the 1st and “bad” PI channels ignored to avoid undesirably influencing the fit. The spectral model is then loaded and fit to the data allowing the line energy normalizations to float (with the exceptions mentioned section 2.2), as well as the SMC component absorption, and the bremsstrahlung temperature and normalization. Please refer to figure 2 for a sample spectral fit of obsid 420.

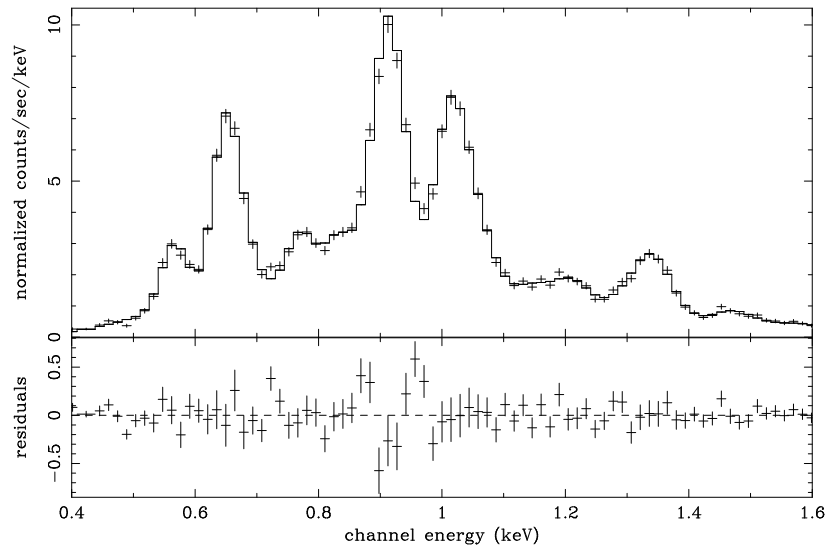


**Figure 2.** Sample linear plot of a spectral fit of obsid 420 taken 14-03-2000 at -7' off-axis. The data plotted here have had CTI-correction and time-dependent gain applied and were fit using reponse products generated by calcarf and calcrmf2.

Once spectral fitting is complete, the *XSPEC* **ERROR** command is issued to determine the 90% confidence error limits. Because the measured flux is dependent on the count rate, the percentage error in the flux and the count rate is the same. This can be used to obtain a rough estimate of flux error by evaluating the ratio of count rate error to count rate and comparing to the measured flux. The differences between the calcarf/rmf and the default arf/rmf fitted data are immediately apparent in the series of plots (Figures 3-5) included in Appendix A which compare pertinent spectral model components and line normalizations for each observation.

### 3.2. ACIS-I Data

In the following section, we refer to the set of Figures 3 to 4 found in the appendix. There are six panels representing various spectral parameters per page. The three left panels show the fit results obtained using the calcarf/rmf response files and the three right panels depict the fit results obtained using the default response products. In addition to this, within each figure, different symbols are used to denote nodes 0-3 on the I3 chip and different levels of grey-scale are used to denote approximate location on the chip (aimpoint=black, mid-chip=medium gray, and framestore=light gray - please refer to the comment on the figure).

#### 3.2.1. Fitted model parameters: Brems and NH

In the middle two panels of Figure 3, one can clearly see that the use of calcrmf and calcarf has significantly reduced the uncertainty in the bremsstrahlung temperature. In addition to this, there appears to be a convergence in the spatial and nodal differences of the fitted temperature value at each set of observations. The average value of the temperature has been slightly reduced when compared to the default fits. Notice in comparing the top two panels in Figure 3 that the bremsstrahlung normalization is consistently higher in the corrected fits, indicating that the absorption by the contaminant has been accounted for in the fit. Again, the uncertainties in these normalization values have been slightly reduced in the calcarf/rmf fits.

The bottom two panels of Figure 3 show a striking difference between the default and corrected fits of the SMC component neutral Hydrogen column density (NH). As one might expect, the default fits show the NH continually rising over time, presumably to account for the increase in absorption caused by the growing layer of contamination. However, in the case of the calcarf and calcrmf fits, it appears that the model may be over-compensating for absorption by the contaminant such that the value of the NH is consistently zero for each observation.

#### 3.2.2. Fitted model parameters: Flux and O & Ne normalizations

The fitted model flux from 0.4 to 2.5 keV is shown in the top two panels of Figure 4. The contamination-corrected results are again repeatedly higher than the default results. Consistent with a time-dependent growth in contamination, the default fits show a decrease in overall flux over time. As evidenced in the calcarf/rmf panel, this effect is mitigated by the contamination model, though the model may underestimate the contaminant at later epochs as there appears to be a slight decrease in flux at the last four epochs.

The middle panels of Figure 4 show that the contamination model increases the O VIII Ly  $\alpha$  normalization at each observation over the default results and the normalizations are fairly uniform over time. It is not immediately apparent that the default fit results show a continuous decrease in O VIII Ly  $\alpha$  normalization over time as would be expected from a continuously increasing contamination layer. The Ne X Ly  $\alpha$  normalization vs time is shown in the bottom panels of Figure 4. The contamination model consistently increases the normalization of this line over the same observation in the default fits. The results are largely consistent over time and across the CCD, agreeing well with the contamination time and spatial dependencies.

### 3.3. ACIS-S Data

Figure 5 in appendix A represents the same set of fitted spectral components as that of I3, however, the visualization of the data is slightly different. Each panel contains the fit results of both the default and calcarf/rmf response products. In each panel, fit results from the default response files are denoted as “CALDB” and represented in light gray. Similarly, fit results from the calcarf/rmf response files with the prototype S3 QE curve are denoted as “CALCARF+newQE” and represented in black. In addition, triangles are used to represent node 1 on the S3 chip and squares represent node 0 (please refer to the comment on the figure about the grayscale).

### 3.3.1. Fitted model parameters: Brems and NH

In the top left panel of Figure 5, the use of calcarf/rmf has raised the overall bremsstrahlung temperature over time and reduced the nodal differences on S3 at most epochs. This parameter is correlated with the overall normalization of the continuum, so the contamination model attempts to reduce the decline seen in the default data. The uncertainties in bremsstrahlung normalization have been reduced in the calcarf/rmf fits, as shown in in the top right panel. As absorption by the contaminant increases over time, the normalization of the default fitted values appears to increase, dramatically in the case of node 0. One can see that the calcarf/rmf data greatly reduce the nodal differences in the bremsstrahlung normalization.

One spectral parameter that can mimick the effect of the contamination is the NH. The middle left panel shows how the default fits continually increase this absorption, effectively accounting for the increased low energy absorption over time. Again, it can be argued that the contamination model is overcorrecting for absorption since the best-fitted NH values tend towards zero.

### 3.3.2. Fitted model parameters: Flux and O & Ne normalizations

The flux versus time plot contained in the middle right panel is perhaps one of the clearest examples of the effect of contamination on the ACIS OBFs. Notice how the flux between 0.4 and 2.5 keV significantly decreases over time in the default data. Using the contamination model, not only has this effect been ameliorated, but the slight nodal differences in flux have been reduced as well. The slightly discrepant, increased flux datapoint around day 1300 is an observation that was taken with a shorter frametime than the rest in this analysis. This reduces the effects of pileup and results in a higher count rate.

It is in the area of the O lines between 560 and 840 eV that the contamination model has a very large effect on the line normalizations. The bottom left panel shows that the O VIII Ly  $\alpha$  fits using the contamination model are more consistent in normalization, and less uncertain than their default fitted counterparts. The Ne lines around 1022 eV are much less sensitive to the absorbing effects of the contamination layer. The bottom right panel shows the energy dependence of the contamination model in that the Ne X Ly  $\alpha$  fitted normalizations using both the default products and the calcarf/rmf products are largely similar.

### 3.4. ACIS-I vs ACIS-S

The apparent discrepancies between observations of the same sources made using FI and BI CCDs on ACIS have also been a focus of ACIS calibration. As an additional aspect of this analysis, a new prototype quantum efficiency QE curve for the BI CCD S3 has been used in the generation of response files incorporating the contamination model. We find that, with contamination correction applied to both FI and BI data, the prototype QE brings some of the results of these two CCDs even closer together. More specifically, with all corrections applied, one can see in comparing the fitted normalizations of Ne X Ly  $\alpha$  in Figures 4 and 5 that they agree rather well between the FI and BI CCDs. The OVIII Ly  $\alpha$  fitted normalizations in the same two figure also agree between the two CCDs, though node 1 on S3 appears to have a slightly lower normalization than those on I3. Taking into account that the error bars on the flux measurements are likely underestimated, it also appears that the flux as measured between 0.4 and 2.5 keV on both S3 and I3 agree in the top left panel of Figure 4 and middle right panel of Figure 5.

Though the fitted line normalizations and flux agree between FI and BI CCDs, there are noticeable differences in the fitted values of the thermal bremsstrahlung temperature, kT, and its normalization. It is difficult to compare the fitted NH results at this point since the model may overcorrect for the contamination on both CCDs as the NH is consistently zero. The BI S3 CCD, which generally receives more incident background flux than its FI counterpart, shows a consistently lower bremsstrahlung normalization but a higher fitted kT value than I3. It is known that the contamination model on S3, at this time, becomes unreliable below  $\approx 0.5$  keV. This limitation of the model could have an effect on the fitted values of the bremsstrahlung normalization and temperature. Slight

uncertainties in the low and high energy extremes of the E0102 spectrum can greatly influence the outcome of these two parameters.

#### 4. CONCLUSIONS

We have analyzed 62 observations of the SMC supernova remnant E0102 on the ACIS I3 and S3 chips, at varied locations, and spanning over 4 years, in an effort to verify the spatial and temporal dependence of the ACIS contamination model. We find that this model alleviates the most egregious effects of the contamination very well on both chips, however a higher-fidelity model of the composition of the contaminant, its spatial distribution and its deposition rate over time might be needed to resolve issues raised in this analysis. Those issues include the possible underestimation of the time dependence and the low-energy uncertainties in the model. We also note that further investigation is required to resolve the discrepancies in results obtained using FI vs BI CCDs. The continued vigilant calibration of both the contamination layer and the ACIS CCDs will certainly play a major role in the continued success of this mission. With the latest peer review cycle having just been completed, AO6 will be full of many diverse observations further advancing astronomy today and into the future.

#### ACKNOWLEDGMENTS

The authors would like to acknowledge the help and support of the *Chandra* community, particularly members of the Chandra X-ray Center (CXC) for their pertinent discussions and suggestions. The Chandra X-ray Center is operated for NASA by the Smithsonian Astrophysical Observatory under contract NAS8-39073.

#### REFERENCES

1. P. P. Plucinsky, N. S. Schulz, H. L. Marshall, C. E. Grant, G. Chartas, D. Sanwal, M. Teter, A. A. Vikhlinin, R. J. Edgar, M. W. Wise, G. E. Allen, S. N. Virani, J. M. DePasquale, and M. T. Raley, "Flight spectral response of the ACIS instrument," in *X-Ray and Gamma-Ray Telescopes and Instruments for Astronomy*, Joachim E. Truemper, Harvey D. Tananbaum, eds., *Proc. SPIE*, **4851**, pp. 89-100, 2003.
2. H. L. Marshall, C. E. Grant, A. P. Hitchcock, S. O'Dell, and P. P. Plucinsky, "Composition of the Chandra ACIS contaminant," in *X-Ray and Gamma-Ray Instrumentation for Astronomy XIII*, K.A. Flanagan and O.H.W. Siegmund, eds., *Proc. SPIE*, **5165**, pp. 497-508, 2004.
3. A. Vikhlinin, "Spatial structure in the ACIS OBF contamination," *CXC internal memo*, May 9, 2004.
4. K.A. Flanagan, C.R. Canizares, D. Dewey, J.C.Houck, A.C. Fredericks, M.L. Schattenburg, T.H. Market, D.S. Davis, 2004, *ApJ*, 605, 230
5. A.P. Rasmussen, E. Behar, S.M. Kahn, J.W. den Herder, K. van der Heyden. 2001, *A&A*, 365, L231

#### APPENDIX A. FIGURES

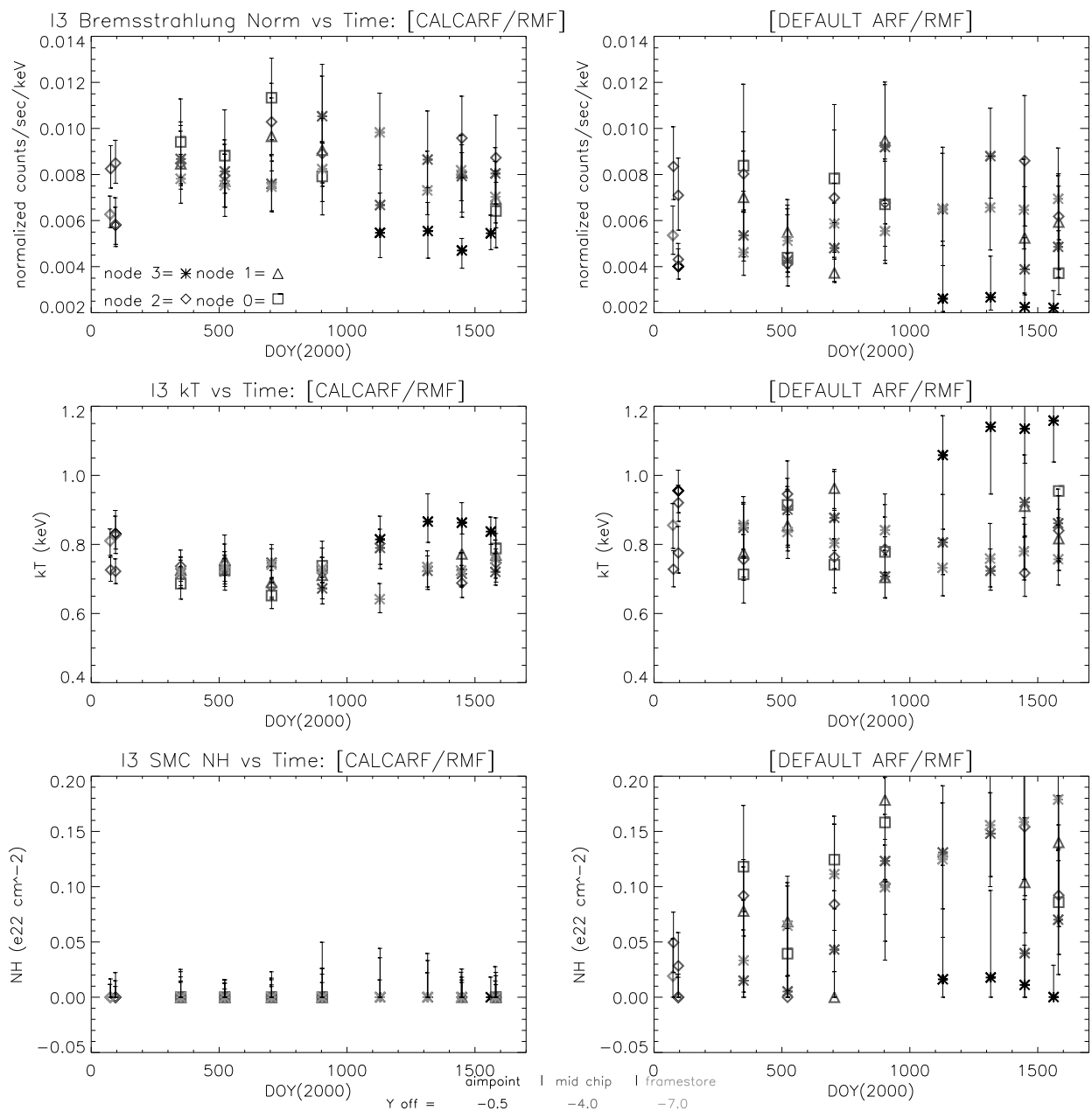


**Figure 3.** This figure contains 6 panels of E0102 ACIS-I3 fitted spectral parameters plotted versus time. Each set of two panels compares the calcarf/rmf results (left) to the default response results (right). The top two panels depict the bremsstrahlung normalization versus time, while the middle two show the kT value and the bottom two contain the SMC component absorption versus time. Symbols are used here to represent different nodes; node 0 is represented by a square, node 1 by a triangle, node 2 by a diamond and node 3 an asterisk. Grayscale is used to denote approximate chip location with black denoting near aim point observations, medium gray denoting mid-chip observations and light gray denoting observations near the framestore.

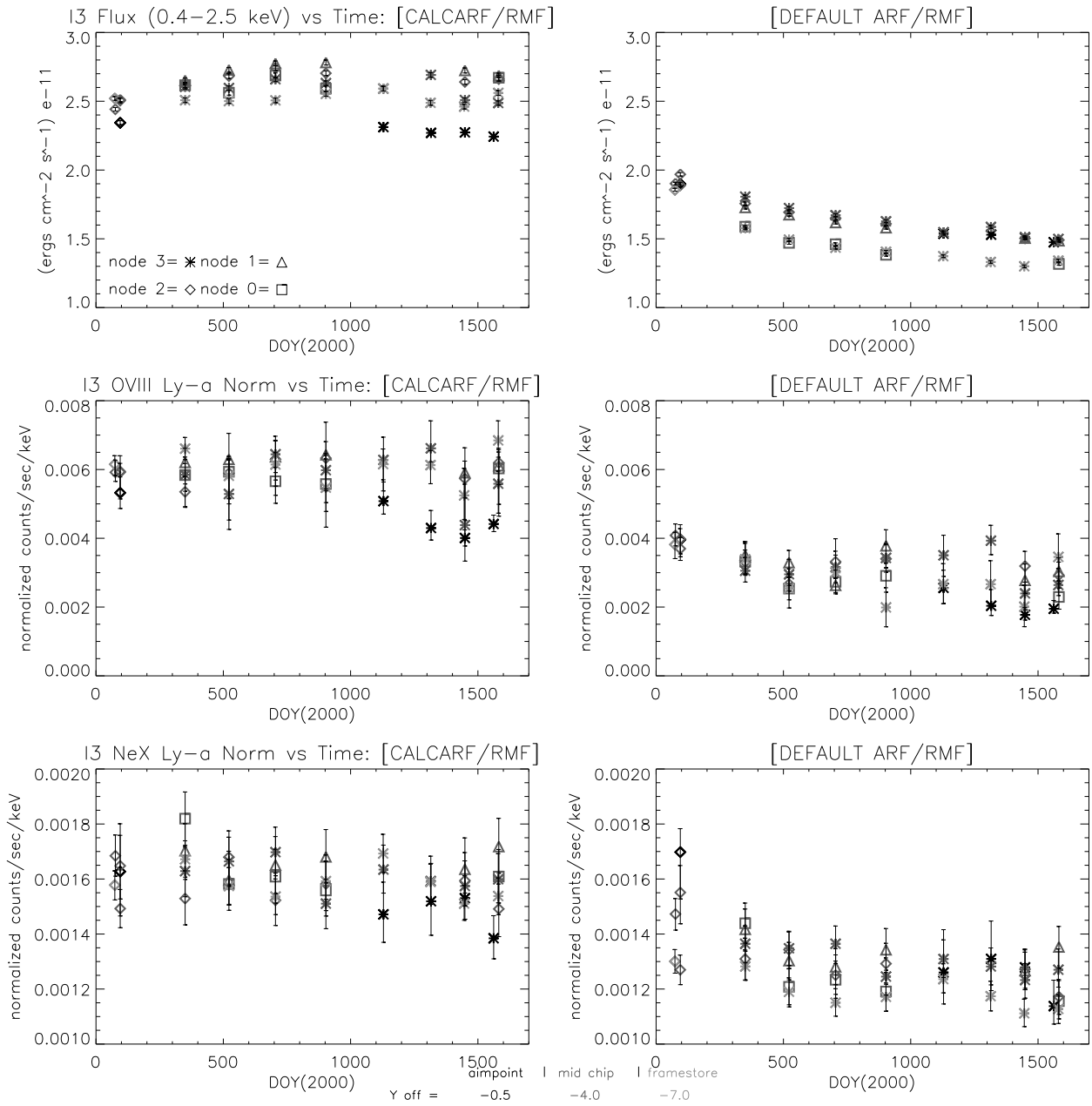


**Figure 4.** This figure contains 6 panels of E0102 ACIS-I3 fitted spectral parameters plotted versus time. Each set of two panels compares the calcarf/rmf results (left) to the default response results (right). The top two panels depict the the model flux from 0.4 to 2.5 keV versus time, while the middle two show the the OVIII Ly  $\alpha$  normalization versus time and the bottom two contain the Ne X Ly  $\alpha$  normalization versus time. Symbols are used here to represent different nodes; node 0 is represented by a square, node 1 by a triangle, node 2 by a diamond and node 3 an asterisk. Grayscale is used to denote approximate chip location with black denoting near aim point observations, medium gray denoting mid-chip observations and light gray denoting observations near the framestore.

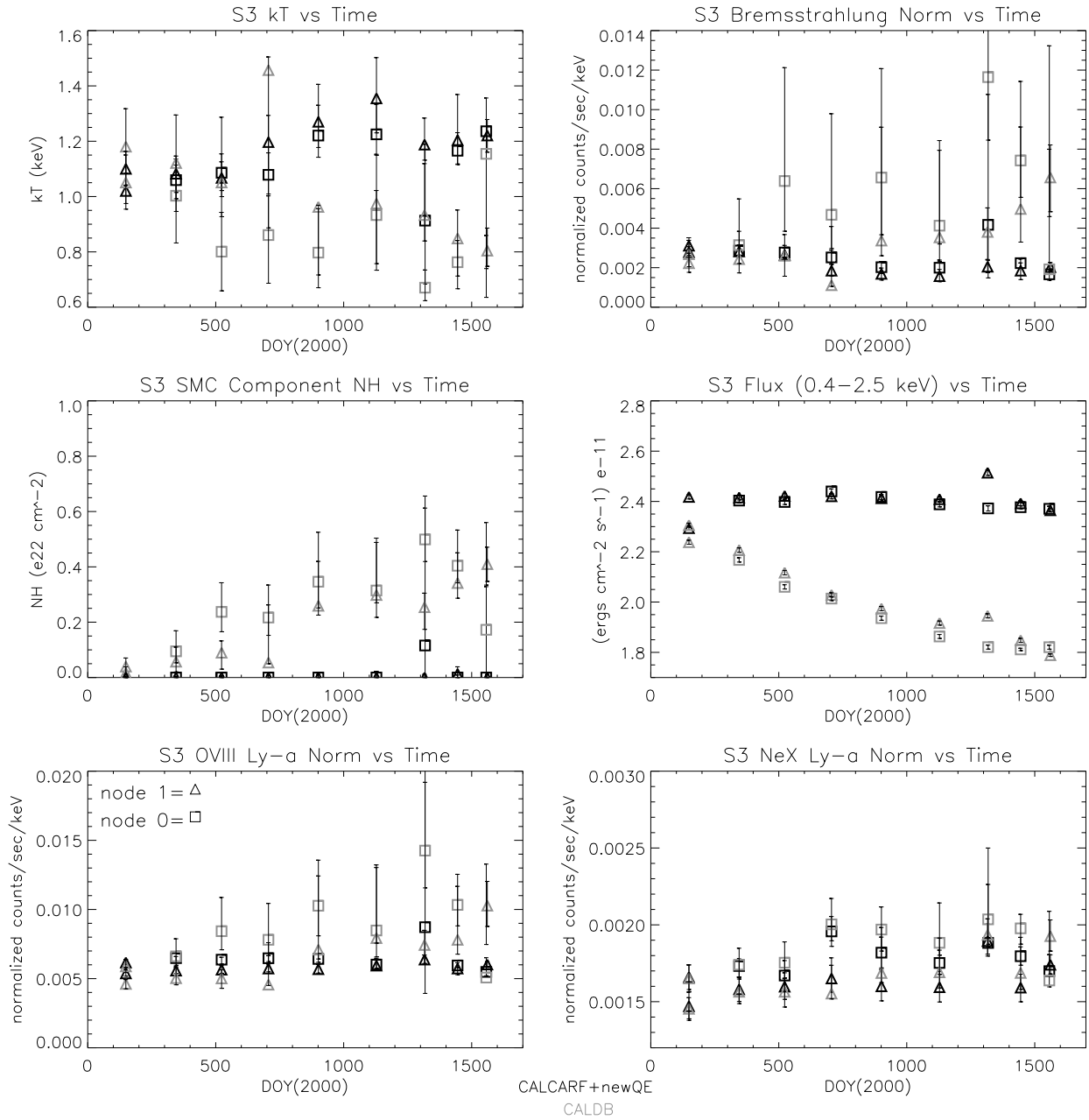


**Figure 5.** This figure contains 6 panels of E0102 ACIS-S3 fitted spectral parameters plotted versus time. Each panel, however, depicts a different parameter with the default and calcarf/rmf response results plotted in the same panel. The top left panel shows the fitted kT value versus time, while the top right shows the bremsstrahlung normalization versus time. The middle panels show the SMC component absorption versus time on the left and the flux from 0.4 to 2.5 keV versus time on the right. The bottom two panels show the fitted line normalizations versus time of OVIII Ly  $\alpha$  (left) and Ne X Ly  $\alpha$  (right). Two symbols are used to represent the nodal locations of these observations; node 0 is represented by a square, while node 1 is represented by a triangle. Grayscale is used to show the two types of response products used with black denoting the calcarf/rmf results and light gray denoting the CALDB default results.